PHYSICAL REVIEW B VOLUME 37, NUMBER 18 15 JUNE 1988-II

Far-infrared and electrical transport studies of oxide-charge-induced localized states in a quasi-two-dimensional system

E. Glaser* and B. D. McCombe

Department of Physics and Astronomy, State University of New York at Buffalo, Buffalo, New York 14260

(Received 22 September 1987; revised manuscript received 1 February 1988)

Far-infrared measurements of intersubband absorption spectra and dc electrical transport studies of *n*-type inversion layers in (100) Si metal-oxide-semiconductor field-effect transistors with mobile positive ions in the oxide have been performed at temperatures between 1.7 and 80 K. The properties of the electronic states in the quasi-two-dimensional conducting layer of the MOS devices were probed in detail by conductance, capacitance, and transconductance measurements, and by intersubband infrared optical-absorption measurements. Data were obtained with positive oxide charge density as a parameter, varied by drifting controlled amounts of positive ions (ΔN_{ox}) to the oxide-semiconductor interface ($1.3\times10^{11}\leq\Delta N_{ox}\leq7.0\times10^{11}$ cm^{-2}). These results were compared with similar measurements on high-mobility devices in which no positive impurity ions have been purposely introduced. Studies were carried out over a wide range of *net* interfacial oxide charge densities ($2\times10^{10}\leq N_{ox}\leq1\times10^{12}$ cm^{-2}) and substrate-source bias voltages ($-9\leq V_S\leq1$ V) with the goal of attaining a better understanding of the nature of localization effects (e.g., two-dimensional carrier localization), interface scattering, and many-body Coulombic interactions (e.g., screening effects) in these structures. Results are compared with recent experimental investigations of this and similar systems and with predictions of available theoretical models. The present measurements provide evidence for the existence of impurity bands and long band tails at low electron densities ($n_s\leq N_{ox}$) associated with subbands due to both the inequivalent conduction-band valleys and for *screening* of these localized states at high electron densities ($n_s\geq2N_{ox}$).

I. INTRODUCTION

Over the past few years there has been much interest in systems of reduced dimensionality in which charge carriers are confined to the vicinity of junctions between insulators and semiconductors or between layers of different semiconductors. The motion of charge carriers in such systems is constrained in the direction perpendicular to the interface by built-in or applied electric potentials while motion parallel to the interface is unconstrained. Experimental investigations coupled with theoretical calculations have demonstrated the dynamically two-dimensional (2D) behavior of carriers (electrons or holes) in the plane of the interface (see Ref. 1 for a comprehensive review of the electronic properties of two-dimensional systems). In addition, it has been shown recently that the electrical and optical properties of charge carriers located at or near semiconductor interfaces are strongly affected by the presence of impurities.[2–4] These effects include 2D carrier localization, interface scattering, and many-body Coulombic interactions (e.g., screening effects). A unique and powerful tool for investigations of these effects in quasi-two-dimensional systems is provided by Si metal-oxide-semiconductor field-effect transistor (MOSFET) devices whose oxides are intentionally doped with positive ions. The MOS device is well suited for such investigations because several important parameters can be varied independently and determined with reasonable precision; the number density of carriers in the space-charge layer, the number density of charged impurities near the interface (the oxide charge density), and the average "distance" of the space-charge carriers from the semiconductor-insulator interface.

The present work offers a combination of far-infrared optical and dc electrical-transport measurements to probe this system of electrons in the presence of charged impurities in the oxide. The dc electrical-transport studies include conductance, transconductance, and capacitance measurements at low temperatures (1.7–77 K) on Si MOS devices with mobile positive ions deposited in the oxide and with "clean" oxides. In addition, far-infrared optical measurements were made via Fourier-transform spectroscopic techniques at 4.2 K and above on the same samples in order to study the subband energy structure of the confined carriers with positive oxide charge density as a parameter.[5] The present measurements provide significant optical evidence for the existence of impurity bands and for screening of these localized states in 2D systems. In Sec. II the significant results of recent experimental and theoretical investigations of Si MOSFET device structures with mobile positive ions in the oxide are reviewed. In Sec. III, a brief description of the electrical-transport measurement techniques and of the sample-mounting arrangement, coupling scheme, and gate-modulation technique employed to obtain the infrared data is given. In Sec. IV we present the results of the electrical-transport and far-infrared optical measurements and summarize general features and trends. In Sec. V, a discussion of the significance of these results and comparison with results of recent experimental investigations of this and similar systems and with predictions

of available theoretical models is made. A summary and overall conclusions of this work are offered in Sec. VI.

II. EXPERIMENTAL BACKGROUND AND MODELS

A major experimental advantage of a Si MOSFET device with mobile positive ions in the oxide is the ease with which controllable amounts of positive ions can be drifted under an applied gate voltage to the oxide-semiconductor interface and "frozen" in place at reduced temperatures. At sufficiently low densities, those ions near the interface can lead to discrete bound states occupied by inversion-layer electrons.[6] However, in general, the density of electron states $[\rho(E)]$ in a real system averaged across the surface is difficult to model. The ideal density of states per unit energy per unit area for the quasi-two-dimensional inversion-layer system is altered in the presence of random surface potential fluctuations. Oxide charge near the Si/SiO_2 interface and the nonuniformity of the Si/SiO_2 interface itself can *both* contribute to potential fluctuations. These potential fluctuations will result in regions, randomly distributed laterally both in position and size, of potential minima where electrons can be trapped. The two-dimensional density of states averaged over the surface no longer takes the form of a step function with onset at the subband bottoms, but is pictured to include a "tail" of states which extends to energies below the usual subband edge.[6] In terms of the model proposed by Mott,[7] a mobility edge, E_c, is defined as an approximate energy marking the boundary between localized electron states [whose wave functions parallel to the surface decay as $\exp(-\alpha r)$, where r is measured with respect to the impurity-site location and α is the inverse localization length] and electrons in extended states (however, with short mean free paths). Below the mobility edge electrons can only move by thermally activated tunneling or hopping to other sites, or by thermal excitation to extended states above the mobility edge. In addition, for a sufficiently high interfacial positive ion density, a *band* of impurity states which lies at energies distinctly below the band tail is expected to be formed due to wave function overlap. This picture assumes that the "impurities" are all located in a narrow range of distance from the interface.

Evidence for the existence of 2D impurity bands was obtained initially by Fowler and Hartstein[8] via low-temperature transport studies on (100) Si MOS n-type inversion-layer devices with mobile Na^+ ions in the oxide. Above a minimum value of interfacial oxide charge density, a conductance peak was observed before the sharp onset of conduction. The conductance peak was attributed to the existence of a band of localized states below the lowest electric field subband in the silicon. The maximum of this peaked structure was assumed to correspond to the maximum in the density of states of a half-filled, nondegenerate, sodium-derived impurity band [since σ is proportional to $\rho(E_F)$, the density of states at the Fermi level]. Such structure has been reported *only* in sodium-doped MOS devices. Recently, Timp *et al.*[9] have extended these dc transport experiments over a wider range of impurity-concentrations ($2\times 10^{11} < N_{ox} < 1.1\times 10^{12}$ cm^{-2}) and temperatures (380 mK $< T <$ 80 K). These results support the earlier interpretation of the low-temperature electrical-transport data in terms of impurity bands.

The limiting case of one electron bound to a single positive charge in the presence of a semiconductor-insulator interface and an electric field has been studied extensively.[10–12] These theories differ in the degree of sophistication of the variational trial wave functions employed to describe the electronic motion. Estimates of the binding energy for the ground state with the impurity ion located at the interface have been reported by these authors to lie in the range 25–30 meV (measured with respect to the lowest subband edge) for experimentally realized values of electric fields (10^4–10^5 V/cm).

In actual Si MOS devices the electron concentration can be controlled over a wide range ($< 10^{11}$–10^{13} cm^{-2}) of values. Thus, this system provides a useful tool for a study of the effects of mutual Coulomb interactions, especially screening effects. For example, the situation in which the number density of inversion-layer electrons is *much larger* than the number density of interfacial impurity ions has been studied theoretically.[13,14] In Ref. 13 it was assumed in this high-density limit that the impurity potential is completely screened out within the distance between impurities. The Kohn-Sham local-density functional method[15] was employed to calculate the screened potential self-consistently. It is found that the bound level is fourfold degenerate (surprisingly) and, as expected, is quite shallow (e.g., binding energy ~ 0.4 meV for $n_s = 4\times 10^{12}$ cm^{-2}).

In addition to impurity-state binding energies associated with the lowest-lying electric subband ($n = 0$), Kramer and Wallis[16] have calculated binding energies of impurity states associated with higher subbands. These authors find that the calculated impurity-derived intersubband transition energies between the lowest-lying bound states connected with the ground ($n = 0$) and first-excited ($n = 1$) subbands are shifted to higher energies over a wide range of electric fields compared to the continuum transitions. The shift in transition energy is consistent with the impurity state for the higher subband being less tightly bound than the ground impurity state associated with the lowest subband, since the Coulombic attraction experienced by electrons in impurity states associated with higher subbands is not as strong as that for electrons located deeper within the potential well with wave function peaked closer to the interface.

Evidence from far-infrared spectroscopic studies for shifted intersubband transitions in the presence of positive oxide impurities was reported initially by McCombe and Schafer.[3] A large shift ($\sim$3–4 meV) to higher energies of the $0\rightarrow 1$ continuum intersubband transition above a minimum value of N_{ox} was observed, qualitatively consistent with calculations by Kramer and Wallis of intersubband transitions in the presence of isolated positive ions. The calculated shift in energy for positive ions at the interface was approximately twice the experimentally observed shift.

Recent experimental investigations[4,17] of the frequency dependence of the dynamical conductivity for electronic

motion parallel and perpendicular to the Si/SiO_2 interface in n-type accumulation-layer devices ($N_{depl} \cong 10^{10}$ cm^{-2}) in the presence of interfacial Na^+ ions coupled with theoretical calculations[18] have questioned the interpretation in terms of impurity bands for the results of the previously described low-temperature dc transport and far-infrared intersubband spectroscopic experiments performed on n-type inversion-layer devices. These authors assert that the same frequency-dependent relaxation function (memory function), $M(\omega)$, employed successfully to describe (in the absence of an impurity band) transport relaxation in the plane of the two-dimensional layer, can account for the experimentally observed broadening and shift of the subband excitation spectrum $[\tilde{\sigma}_{zz}(\omega)]$ in the presence of substantial random positive charge in the oxide near the interface. The predictions of this model are examined in the context of the present experiments in Sec. V.

III. EXPERIMENTAL DETAILS

A. Sample characterization and transport measurements

The Si MOSFET's investigated in this work were large (2.5×2.5 mm^2) thick-gate MOSFET's fabricated on 20-(Ω cm) p-type (100) Si substrates with mobile positive ions deposited in the oxide (sample 1, gate-oxide thickness ~ 1400 Å) and with "clean" oxides (sample 2, gate-oxide thickness ~ 2000 Å). The positive interfacial oxide charge concentration in these samples was varied by the application of positive gate voltages (~ 5–10 V) up to a minute in duration at room temperature to drift a fraction of the positive ions through the oxide from the metal-gate–insulator region to the Si/SiO_2 interface. [The expression "oxide charge density" will always refer to the *number* density (per unit area) of positive ions located in the oxide in close proximity to the Si/SiO_2 interface. This value is given as an equivalent sheet density of charge located *at* the interface.] The experimental probe was then cooled to liquid-nitrogen temperatures with the voltage applied; at this temperature the positive ions are effectively "frozen" in place.

A close approximation to the "true' threshold voltage for conduction in the lowest quasi-two-dimensional subband at various values of the net interfacial oxide charge density for these devices was obtained from conductance–versus–gate-voltage as well as capacitance–versus–gate-voltage measurements at liquid-nitrogen temperatures. From these measurements one can obtain the effective two-dimensional inversion-layer electron-density (n_s) –gate-voltage relationship:

$$n_s=\frac{C_{ox}}{qA}(V_g-V_{th})=\frac{\varepsilon_{ox}}{qd_{ox}}(V_g-V_{th}),\quad V_g>V_{th}\ , \tag{1}$$

where C_{ox} is the gate-oxide capacitance, A is the gate area, d_{ox} is the gate-oxide thickness, and V_g is the voltage applied between the metallic gate electrode and Si substrate. The number density of positive ions drifted to the Si/SiO_2 interface (ΔN_{ox}) is determined, with reasonable precision, from the corresponding *shift* in threshold voltage from

$$\Delta N_{ox}=\frac{\varepsilon_{ox}}{qd_{ox}}[V_{th}(\Delta N_{ox}\neq 0)-V_{th}(\Delta N_{ox}=0)] \tag{2}$$

$$\equiv\frac{\varepsilon_{ox}}{qd_{ox}}\Delta V_{th}\ . \tag{3}$$

In addition, the number density of residual, fixed positive interfacial oxide charge (Q_{SS}) must be included in the determination of the *total* number density of positive interfacial oxide charge (N_{ox}). This contribution (Q_{SS}) is taken conventionally as an average over the oxide thickness set equal to an effective 2D sheet charge *at* the interface. Thus, the total number density of positive interfacial oxide charge is given by

$$N_{ox}=\Delta N_{ox}+Q_{SS}\ . \tag{4}$$

Q_{SS} is calculated from the measured threshold voltage with mobile positive ions drifted away from the oxide-semiconductor interface, combined with measured maximum depletion charge and oxide thickness, calculated Fermi energy in the bulk Si, and literature values of the metal-semiconductor work function. A summary of the pertinent parameters of the devices investigated in this work is presented in Table I.

The transport techniques employed to characterize these devices include conductance, capacitance, and transconductance measurements. All of these techniques make use of a small ac modulation voltage and detect synchronously the output signal with a current sensitive preamplifier–lock-in amplifier arrangement. The applied source-drain voltages was kept small (~ 3 mV) to operate in the Ohmic region of the I_{DS}-versus-V_{DS} curves and to avoid electron-heating effects.

The channel conductance was determined from two-terminal source-drain current–versus–gate-voltage measurements with an ac source-drain voltage of 3 mV rms at 1000 Hz. The threshold voltage was determined from the I_{DS}-V_g curve obtained at 77 K by a straight-line extrapolation to zero conductance near the turn-on region. The low-temperature effective mobility is obtained from the conductance measurements from

$$\mu_{eff}=\frac{\sigma}{C_{ox}(V_g-V_{th})}=\frac{\sigma}{n_s e}\ , \tag{5}$$

where σ is the small-signal sheet conductivity.

An independent determination of the device threshold voltage at 77 K can be obtained from the position in gate voltage at which the capacitance-voltage curve has maximum slope; this corresponds to the onset of strong inversion. In addition, the maximum-depletion charge density, $(Q_{SD})_{max}$, can be obtained[19] from measurements of C_{min}/C_{ox} and C_{ox}. The shape of the C-V_g curves also

TABLE I. Parameters of the devices investigated.

Sample	Device designation	d_{ox} (Å)	N_{depl} (cm^{-2})	Q_{SS}/q (cm^{-2})
1	NASI-3	1400	$(1\pm 0.2)\times 10^{11}$	$(1.3\pm 0.2)\times 10^{11}$
2	ALMOS56A-3	2000	$(1\pm 0.2)\times 10^{11}$	$\leq 2\times 10^{10}$

provides an indicator of macroscopic lateral inhomogeneities associated with the interfacial oxide charge for the samples in which positive ions were drifted purposely to the Si/SiO_2 interface. The symptoms[20] of such charge nonuniformities along the Si/SiO_2 interface plane are a broadening (stretchout) of the C-V_g curves along the gate-voltage axis near the minimum and an increase in the value of $C_{\min}$.

An additional technique employed to characterize the devices was measurement of transconductance (g_m). In this technique a constant (dc) voltage, V_{DS}, is applied between the source and drain contacts, and a small ac signal (<10 mV) is superimposed on the gate voltage. The source-drain ac current synchronous with the gate modulation was measured with a current sensitive preamplifier–lock-in amplifier arrangement. The lock-in amplifier–derived dc signal is proportional to the differential change in channel conductance with respect to small variations in the applied gate voltage,

$$g_m = \left.\frac{d\sigma}{dV_g}\right|_{V_g = V_{DS}} . \tag{6}$$

Weak structure in the channel-conductance measurements ($I_{DS} - V_g$) is more readily observable via transconductance. Also, a second convenient measure of carrier mobility in Si space-charge layers, the field-effect mobility, is provided by these measurements from

$$\mu_{FE} = \frac{g_m}{C_{ox} V_{DS}} . \tag{7}$$

B. Far-infrared optical measurements

The subband-energy structure was probed by means of Fourier-transform spectroscopy (FTS) in conjunction with a Si-prism–coupling scheme and a differential gate-modulation technique. A modified SPECAC model PN 40.000 polarizing Fourier-transform interferometric spectrometer was used for these studies. For the present experiments the system was operated as a conventional Michelson interferometer with a 6-μm Mylar beam splitter. A block diagram of the experimental setup is shown in Fig. 1(a). Light-pipe optics were used throughout; the light was coupled to the sample by means of a special mounting arrangement (discussed below) and, finally, incident on the detector located directly below the sample holder. The light pipe, sample holder, and detector housing unit were surrounded by a 0.5-in.-o.d. thin-wall stainless-steel vacuum jacket filled with low-pressure helium exchange gas for thermal contact.

Since the spectral range of interest for this study was between 80 and 250 cm^{-1}, a gallium-doped germanium (Ga:Ge) photoconductive detector[21] operating at 4.2 K was employed. Cold black polyethylene and single-crystal (c-axis) sapphire filters were placed directly above the detector in order to limit the overall response of the spectrometer system and the background light incident on the detector to frequencies below ~ 300 cm^{-1}. These filters were placed below the sample space since background radiation at energies above 300 cm^{-1} was useful in establishing an equilibrium depletion charge density in these samples.

In order to observe optical intersubband transitions in semiconductor space-charge layers, it is necessary to couple radiation into the inversion layer with the electric field of the incident radiation polarized perpendicular to the Si/SiO_2 interface. A prism-coupling scheme and differential gate-modulation technique[22] was employed to enhance sensitivity in order to observe the weak intersubband transitions in these structures. The technique [see Fig. 1(b)] employs a 45° right-triangular Si prism with the polished Si substrate of the device to be investigated glued backside down to the optically polished long surface of the prism. The unpolarized FIR (far-infrared) radiation is coned-down to a diameter of 2 mm just prior to being reflected from a 45° brass mirror milled into the prism-sample holder. The reflected light is incident normal to one of the small faces of the prism, is totally internally reflected at the Si/SiO_2 interface where it is coupled to the space-charge layer, and subsequently is transmitted out the other small face of the prism and directed to the Ga:Ge detector. A *thick* metal gate electrode in close proximity (~ 1500 Å) to the space-charge layer is important since it shorts out the parallel component of the ir electric field along the Si/SiO_2 boundary: thus this ar-

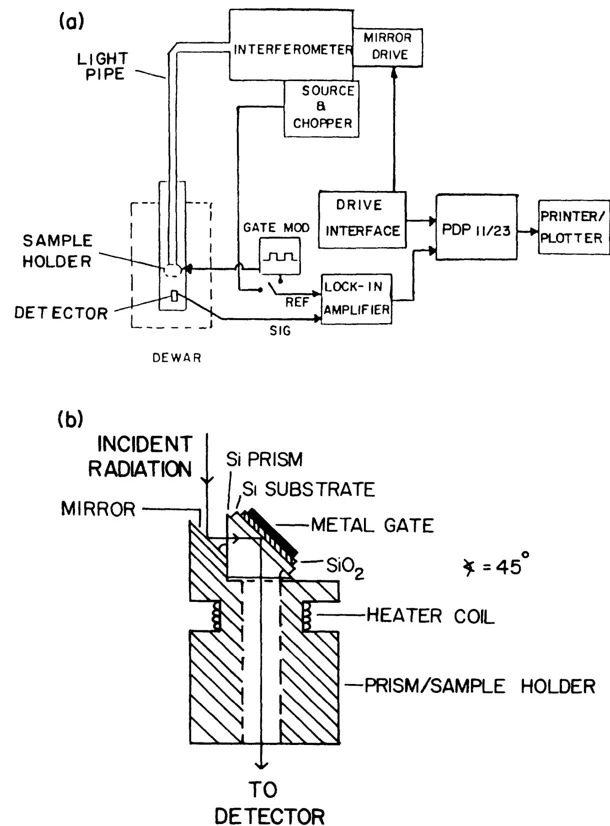

FIG. 1. (a) Block diagram of the FIR Fourier-transform spectrometer system. (b) Configuration employed for coupling FIR radiation into the Si MOSFET with the ir electric field polarized perpendicular to the interface.

rangement acts as a polarizer, coupling the *perpendicular* component of the ir electric field to the n-type inversion layer.

The device gate is square-wave-modulated from a value slightly below threshold ($n_s = 0$) to some desired gate voltage above threshold, which corresponds to a particular n_s given by Eq. (1), at a frequency between 500 and 1500 Hz while the sample is continuously illuminated with ir light from the spectrometer. The resultant amplified detector signal is synchronously demodulated with a lock-in amplifier phase-locked to the square-wave gate modulation. Possible effects of charging time of the inversion layer were checked by varying the gate-modulation frequency over a factor of 30; no change in the peak positions of the subband resonances was observed.

The dc output of the lock-in amplifier is proportional to the difference between the detector signal due to light transmitted through the prism arrangement with no inversion-layer electrons and that transmitted with some desired inversion-layer carrier density. This dc analog signal is digitized, and stored at each discrete value of mirror position to create a digital interferogram. The interferograms are co-added (signal-averaged) for a number of mirror scans, and fast-Fourier-transformed with an on-line microcomputer to obtain the frequency spectrum. This spectrum is normalized to a background spectrum obtained with chopped light; the resultant ratio spectrum is proportional to the absorption coefficient of the inversion layer at a given electron density.

C. Temperature-dependent optical and transport measurements

In addition to measurements obtained at liquid-helium temperatures, optical and transport studies were performed on these samples at elevated temperatures up to 77 K. The sample temperature was determined to within 2 K by means of a Chromel-Constantan thermocouple in thermal contact with the Si prism. Since the conductance of the n-type inversion-layer channel is a strong function of the sample temperature, an excellent independent measure of temperature drift or variation during a multiple-mirror-scan optical measurement was obtained from the conductance–versus–gate-voltage curves before and after the measurement. The I_{DS}-V_g curves were found to be reproducible within the precision of the measurement for each temperature investigated.

IV. RESULTS AND ANALYSES

A. Transport measurements

Initial measurements were carried out on the Si MOS device with mobile positive ions deposited in the oxide (sample 1). Figure 2 summarizes the channel-conductance results obtained at 4.2 K. The effective mobility is plotted versus n_s for four values of ΔN_{ox}. The main qualitative feature of these data to be noted is the substantial decrease in the effective mobility as the oxide charge is increased. The *peak* effective mobility varies from 4400 to 1350 $cm^2/V\,sec$ as N_{ox} varies between 1.3×10^{11} and 7.0×10^{11} cm^{-2}.

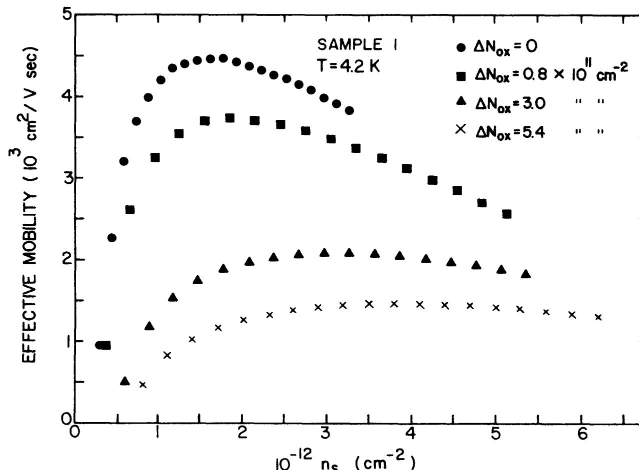

FIG. 2. Effective mobilities vs inversion-layer density at 4.2 K and several values of ΔN_{ox}.

Conductance measurements were also obtained on sample 1 at 4.2 K at densities near threshold by the same ac lock-in technique with *low-frequency* ($f \sim 10$ Hz) source-drain voltages in order to minimize the possible contribution of capacitively coupled currents to the total source-drain current in this region of high channel resistance. Representative conductance curves from sample 1 at 4.2 K under these conditions for a narrow range of gate voltages are shown in Fig. 3 for several values of positive oxide charge density. A conductance peak is observed clearly before the sharp onset of high conductivity

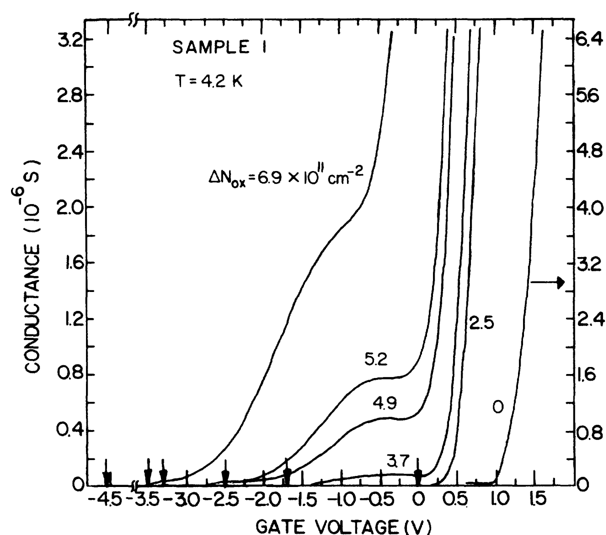

FIG. 3. Conductance vs gate voltage for sample 1 at 4.2 K for several values of ΔN_{ox}. The vertical arrows mark the liquid-nitrogen–temperature threshold voltages for the respective values of ΔN_{ox}. Note the difference in scale for the $\Delta N_{ox}=0$ conductance curve.

for $\Delta N_{ox} \geq 4.0\times10^{11}$ cm^{-2}; it occurs at a gate voltage above the threshold voltage measured at 77 K. For large values of ΔN_{ox} ($\gtrsim 7.0\times10^{11}$ cm^{-2}), the conductance "bump" appears only as a broad shoulder on the channel-conductance curve.

Electrical-transport studies were performed also on Si MOS structures with "clean" oxides (sample 2) to provide a basis for comparison with the results from low-mobility devices. The threshold voltage was found to be $+1.5$ V (± 0.1 V) at 77 K. The peak effective mobility, determined from the conductance data at 4.2 K, occurs at $n_s \cong 7\times10^{11}$ cm^{-2} and is approximately 15 000 cm^2/V sec. This high mobility is evidence of much smaller positive interfacial oxide charge density in these devices, consistent with V_{th}.

Capacitance-voltage measurements were also performed under various conditions to characterize these samples. Typical low-frequency (i.e., gate-voltage-modulation frequency of 1000 Hz) capacitance curves obtained with sample 1 at 77 K are shown in Fig. 4 for several values of ΔN_{ox}. The inversion-layer electron-density–gate-voltage relationship determined from the value of oxide capacitance (C_{ox}) obtained from these results (approximately 1600 pF) is

$$n_s = (1.49\times10^{11})(V_g - V_{th})\ \text{cm}^{-2}\ . \quad (8)$$

As noted in the preceding section, an independent measure of the threshold voltage at 77 K for various positive ion drifts can be obtained from the C-V curves. The value of the position of maximum slope is observed to shift to larger negative voltages (similar to the conductance-threshold measurements) as the interfacial oxide charge density is increased. The position in gate voltage at which the C-V slope is maximum for several positive ion drifts is summarized in Table II. Note that the capacitance thresholds are consistently slightly more negative than the conductance thresholds; the difference *increases* with increasing positive oxide charge, but the threshold determined by the two techniques agrees within the mutual experimental error. The values of ΔN_{ox} can

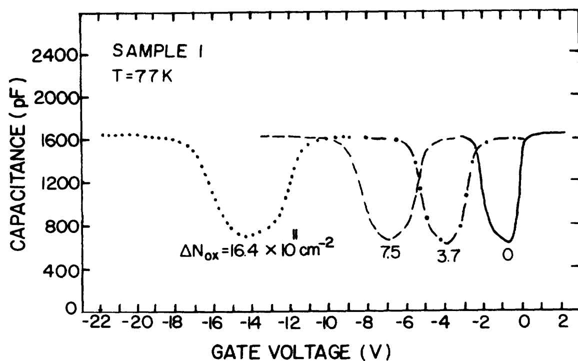

FIG. 4. Capacitance vs gate voltage for sample 1 at 77 K for several values of ΔN_{ox}. Values of ΔN_{ox} are taken from the conductance-voltage threshold measurement.

TABLE II. Threshold voltages (sample 1) from conductance-voltage and capacitance-voltage measurements at 77 K and corresponding values of ΔN_{ox} determined from these measurements.

$(V_{th})_{con}$ (V)	$(V_{th})_{cap}$ (V)	$(\Delta N_{ox})_{con}$ (cm^{-2})	$(\Delta N_{ox})_{cap}$ (cm^{-2})
0.0±0.1	−0.1±0.1	0	0
−0.5±0.1	−0.6±0.2	0.8×10^{11}	0.8×10^{11}
−1.6±0.2	−1.8±0.2	2.4×10^{11}	2.5×10^{11}
−1.8±0.2	−2.0±0.3	2.7×10^{11}	2.8×10^{11}
−2.5±0.2	−2.8±0.3	3.7×10^{11}	4.0×10^{11}
−3.3±0.3	−3.6±0.3	4.9×10^{11}	5.2×10^{11}
−5.0±0.4	−5.4±0.4	7.5×10^{11}	7.9×10^{11}

be determined from the *shift* of the gate voltage for maximum slope from the value observed with the positive ions drifted away from the interface (i.e., $\Delta N_{ox}=0$) or from the *shift* of the conductance onset. There are differences in ΔN_{ox} determined by the two techniques amounting to a maximum of 10%. This is taken to be the uncertainty in ΔN_{ox}. An additional qualitative feature of these results to be noted is the broadening of the C-V_g curves in the vicinity of C_{min} with $\Delta N_{ox}\neq 0$, especially for $\Delta N_{ox} \gtrsim 1\times10^{12}$ cm^{-2}. Furthermore, for $\Delta N_{ox} \gtrsim 1\times10^{12}$ cm^2 the value of C_{min} was observed to increase slightly, indicative of lateral inhomogenities in the oxide charge.

Capacitance-voltage measurements were performed also on the high-mobility device (sample 2). The inversion-layer electron-density–gate-voltage relationship determined from the value of oxide capacitance (approximately 1000 pF) is

$$n_s = (1.00\times10^{11})(V_g - V_{th})\ \text{cm}^{-2}\ . \quad (9)$$

The maximum slope in the C-V curve at 77 K was observed at $V_g = 1.5$ V (in agreement with the corresponding threshold voltage obtained from conductance measurements).

Field-effect–mobility studies as a function of temperature were carried out on the same samples. Measurements on sample 1 for several values of ΔN_{ox} are summarized in Fig. 5. The field-effect–mobility maximum at 4.2 K with the mobile positive ions drifted away from the interface [Fig. 5(a)] shifts to slightly higher gate voltages, broadens substantially, and decreases in amplitude as the sample temperature approaches 77 K. A feature at very low gate voltages appears at $\sim$20 K, and above 40 K it becomes the maximum. Data observed for ΔN_{ox} between 0 and 4×10^{11} cm^{-2} [e.g., Fig. 5(b)] are similar to the results obtained with $\Delta N_{ox}=0$, except the peaked structure at 4.2 K is broader. The results are strongly modified in the presence of *substantial* interfacial oxide charge. Several features are evident above a minimum value of ΔN_{ox} ($\gtrsim 4.0\times10^{11}$ cm^{-2}). As shown in Fig. 5(c) for sample 1 with $\Delta N_{ox} = 4.9\times10^{11}$ cm^{-2}, a peaked structure is observed at 4.2 K at gate voltages below the sharp increase in field-effect mobility. In addition, a second

peaked structure rapidly develops at a higher gate voltage with increasing temperature above 10 K. Note that both of these peaks occur at gate voltages below the usual low-temperature ($T \sim 4.2$ K) field-effect–mobility maximum. Similar structure is observed for slightly larger values of ΔN_{ox} [see Fig. 5(d)].

A summary of the results obtained at $T=10$ K is shown in Fig. 6 for several values of ΔN_{ox}. The second peaked structure clearly develops only above a minimum value of ΔN_{ox}, and its position in gate voltage shifts down with increasing ΔN_{ox}.

Field-effect–mobility measurements as a function of temperature for the high-mobility device (sample 2) are shown in Fig. 7. Structure similar to that for sample 1 with $\Delta N_{ox}=0$ is observed. A feature develops again at low gate voltages (~ 2 V) with increasing temperature above 20 K; it becomes the maximum as the temperature approaches 77 K, but the overall character of the curves is quite different from the results for sample 1.

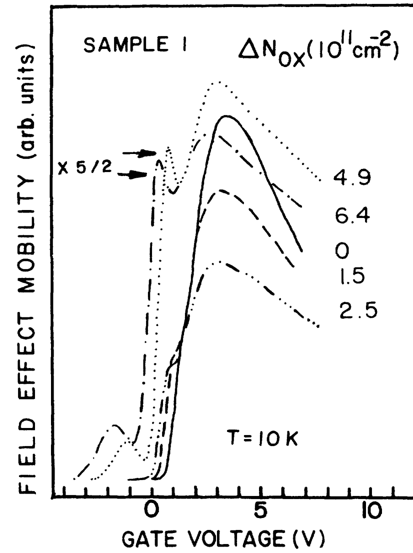

FIG. 6. Field-effect mobility vs gate voltage for sample 1 at $T=10$ K for several values of N_{ox}.

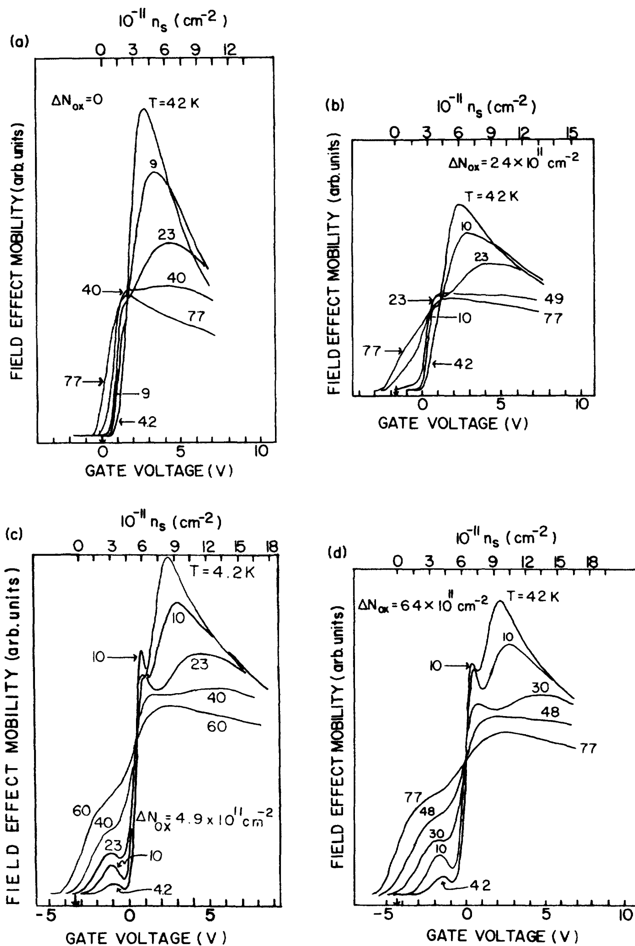

FIG. 5. Field-effect mobility for sample 1 as a function of gate voltage at temperatures between 4.2 and 77 K for several values of positive oxide charge density: (a) $\Delta N_{ox}=0$, (b) $\Delta N_{ox}=2.4$, (c) $\Delta N_{ox}=4.9$, and (d) $\Delta N_{ox}=6.4\times10^{11}$ cm^{-2}. The vertical arrow in each figure marks the liquid-nitrogen-temperature threshold voltage. The corresponding inversion-layer electron densities, determined from the gate voltage *above* the nitrogen-temperature threshold, are shown in the top horizontal axis of each figure.

B. Optical measurements

Far-infrared intersubband measurements were performed on sample 1 at 4.2 K with the mobile positive ions drifted away from the Si/SiO_2 interface region ($\Delta N_{ox}=0$). As mentioned above, the residual postive interfacial oxide charge density (Q_{SS}) for sample 1 was determined to be $(1.3\pm0.2)\times10^{11}$ cm^{-2} and must be in-

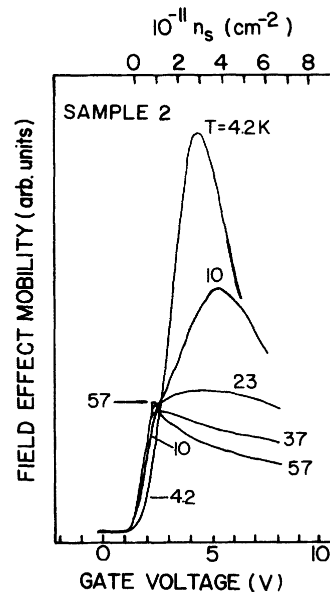

FIG. 7. Field-effect mobility vs gate voltage for sample 2 at temperatures between 4.2 and 77 K. The vertical arrow marks the liquid-nitrogen–temperature threshold voltage.

cluded in the total positive oxide charge density. Representative differential absorption spectra are shown in Fig. 8(a) for several values of inversion-layer electron density (n_s). Two main resonances are observed; the position of the resonance peaks shift monotonically to higher energies with electron density. Note that for a given value of electron density, the intensity of the energetically higher-lying resonance is *much less* than that of the dominant resonance.

The frequency positions of the resonance peaks as a function of electron density are plotted as the solid circles in Fig. 9. The peak energies of the dominant absorption lines appear to correspond to the usual extended-state intersubband transitions between the ground ($n=0$) and first-excited ($n=1$) subbands. The observed $0\rightarrow1$ transition energies are in good agreement with calculated values[23] for the experimentally determined depletion charge density of 1×10^{11} cm^{-2}. Owing to the near cancellation of the depolarization and excitonlike corrections, the transition energies are close to the subband separations over the range of n_s studied. The peak energies of the weak absorption lines are assigned to intersubband transitions between the ground ($n=0$) and second ($n=2$) subbands, though the $0\rightarrow2$ transition energies are not in as good agreement with calculated values (upper solid curve). The disagreement between theory and experiment in this case is not considered significant since the energies of the higher subbands are more sensitive to the value of depletion charge density (uncertain to $\pm15\%$).

For comparison with sample 1, far-infrared optical measurements were also carried out on a sample (sample 2) having a high peak effective mobility. The residual positive interfacial oxide charge density (Q_{SS}) for sample 2 was estimated to be less than 2×10^{10} cm^{-2} from the liquid-nitrogen–temperature threshold voltage. Typical differential absorption spectra obtained at low temperatures are shown for this device in Fig. 8(b) for several values of n_s. Note the narrow absorption linewidths in comparison with the lower-mobility device. The frequency positions of the resonance peaks as a function of inversion-layer electron density for this device are plotted as the open circles in Fig. 9. The peak energies are in good agreement with the calculated values of the $0\rightarrow1$ intersubband transition energies for the experimentally determined depletion charge of 1×10^{11} cm^{-2} ($\pm15\%$)

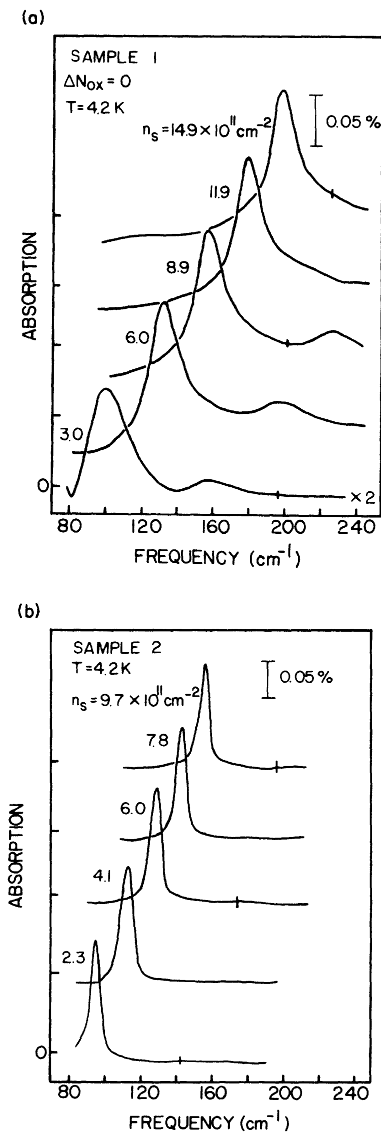

FIG. 8. Differential absorption spectra for several values of inversion-layer electron density (n_s) at $T=4.2$ K for (a) sample 1 with $\Delta N_{\rm ox}=0$, and (b) sample 2. Traces are displaced vertically for clarity. Bars indicate typical noise levels at high frequencies. Noise levels are lower at lower frequencies.

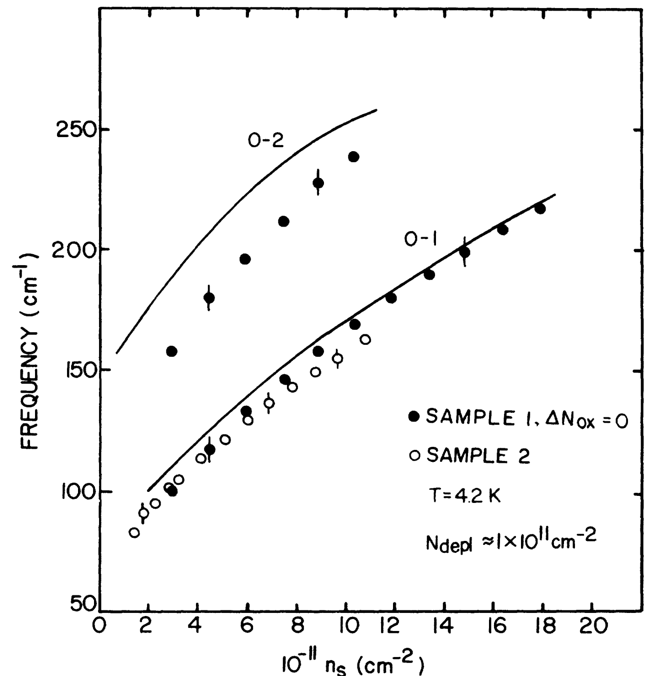

FIG. 9. Compilation of transition energy data vs n_s at $T=4.2$ K for sample 1 with $\Delta N_{\rm ox}=0$ (solid circles) and sample 2 (open circles). The solid lines are theoretical calculations (Ref. 22) for the $0\rightarrow1$ and $0\rightarrow2$ intersubband resonance energies for a depletion charge density of 1×10^{11} cm^{-2}.

and also agree in energy, within the scatter of the data, with the results obtained from sample 1 with $\Delta N_{ox}=0$. Note, however, that the $n=0$-to-$n=2$ subband transition is *not observed,* in contrast to the results obtained for sample 1.

The effects of positive interfacial oxide charge impurities on the optical intersubband transitions at 4.2 K in these devices are shown in the differential absorption spectra of Fig. 10. Data are presented for a low (as described below) value of n_s and several values of interfacial oxide charge density. Several features are evident. The peak position of the dominant absorption peak is independent of drifted positive oxide charge density between $\Delta N_{ox}=0$ and $\Delta N_{ox} \lesssim 4\times10^{11}$ cm^{-2}, but the lines broaden significantly with oxide charge for this range. The line shifts *abruptly* to higher frequencies above 4.0×10^{11} cm^{-2}, and for ΔN_{ox} greater than this the *position* of the shifted resonance peak is *independent* of interfacial oxide charge, up to and including the maximum drifted positive ion density investigated. In addition, there is a significant loss of integrated intensity (factor of ~5.5) of the absorption lines at these low values of electron density for $\Delta N_{ox} \gtrsim 4.0\times10^{11}$ cm^{-2}. For $n_s \geq 10^{12}$ cm^{-2} and $\Delta N_{ox} < n_s/2$ the $0\rightarrow1$ absorption lines broaden substantially with increasing ΔN_{ox}, while the peak positions are essentially independent of ΔN_{ox}. However, the integrated intensity of the $0\rightarrow1$ absorption is *independent* of N_{ox} within experimental error ($\pm20\%$).

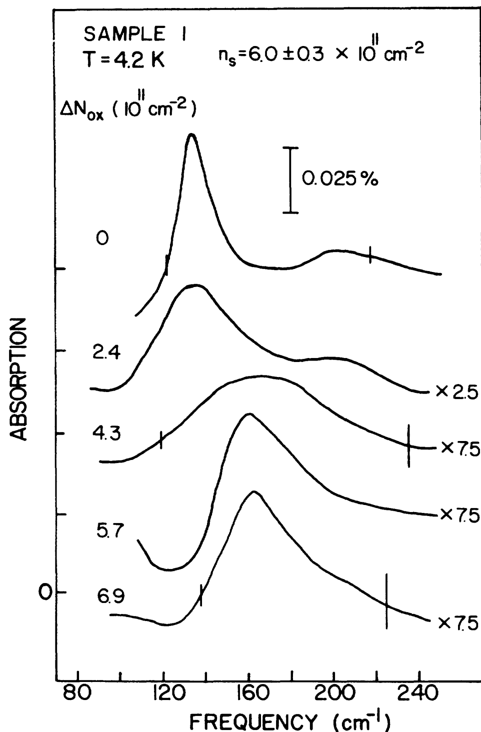

FIG. 10. Differential absorption spectra for sample 1 at $T=4.2$ K for a "low" value of carrier concentration (as described in text) and several values of interfacial oxide charge density. Bars indicate typical noise levels of these data at both low and high frequencies.

A compilation of the transition energy data[5] for sample 1 as a function of electron density for several values of ΔN_{ox} is shown in Fig. 11. As noted above, at the lowest values of N_{ox} obtainable in these samples with mobile positive ions in the oxide, absorption lines are observed whose peaks agree in energy with those calculated for the usual extended state $0\rightarrow1$ intersubband transitions. Up to a minimum positive interfacial oxide charge density [$N_{ox}\sim(3-4)\times10^{11}$ cm^{-2}], the peaks of the observed transition resonances agree in energy within experimental error with the results obtained for $\Delta N_{ox}=0$ over the entire range of n_s investigated. Above a minimum value of interfacial oxide charge density, and over a range of (low) inversion-layer electron densities ($n_s < N_{ox}$), the absorption lines are *all* shifted to higher energy by about 4 meV, *independent* of ΔN_{ox} between 4.3×10^{11} and 6.9×10^{11} cm^{-2}. As n_s is increased beyond N_{ox}, the transition energies of the shifted lines approach the $\Delta N_{ox}=0$ ($0\rightarrow1$) "subband" transition energy curve, and are coincident with this curve within experimental error for n_s greater than approximately $2N_{ox}$.

Intersubband resonance studies were also performed with negative substrate-source bias voltages ($V_S<0$). The equilibrium depletion charge density increases under such conditions according to

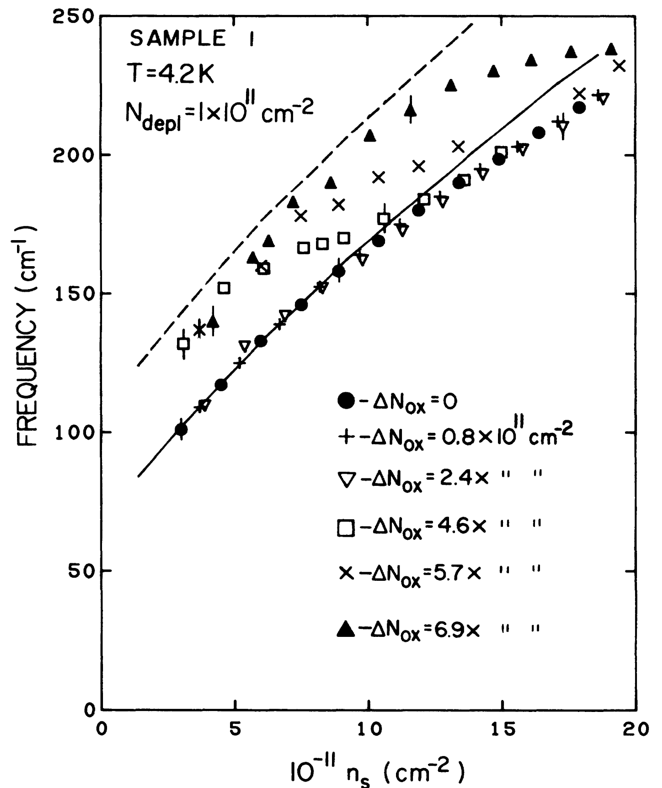

FIG. 11. Compilation of transition energy data for sample 1 at $T=4.2$ K as a function of n_s for several values of ΔN_{ox}. The solid line is a fit to the observed continuum transition energies. The dashed line results from calculation of the impurity-derived intersubband transitions ($2p_0$-like) with the oxide impurity ion located 11 Å away from the ideal Si/SiO_2 interface.

$$N_{\text{depl}}(V_S)=N_{\text{depl}}(V_S=0)\left[\left[1-\frac{V_S}{1.1}\right]^{1/2}\right],\quad V_S<0\ . \tag{10}$$

Hence, the subband energy structure of the n-type inversion layer will be modified since the effective surface electric field (F_S) increases with N_{depl}; the resultant subband energy separations will increase with $V_S<0$ at constant n_s. A summary of the transition energy data as a function of electron density with $V_S=-3V$ [$N_{\text{depl}}=2N_{\text{depl}}(V_S=0)$] is shown in Fig. 12 for $\Delta N_{\text{ox}}=0$ and 4.5×10^{11} cm^{-2} along with the results obtained with $V_S=0$ V (solid symbols). The $0\rightarrow1$ intersubband transition energies (solid circles) shift to higher frequencies, as expected, with increasing depletion charge density. The transition energies at low n_s with $V_S=-3$ V (open circles) again shift to higher energies for $\Delta N_{\text{ox}}\geq4.0\times10^{11}$ cm^{-2} and, furthermore, approach the continuum subband curve at high n_s. There is no significant difference in the value of n_s at which the $\Delta N_{\text{ox}}>0$ curves become coincident with the $\Delta N_{\text{ox}}=0$ curves in the two cases.

In order to investigate further the nature of the optical transitions in this system, the temperature dependence of the intersubband transitions was studied over a range of values of N_{ox}. Temperature-dependent studies on sample 1 with $\Delta N_{\text{ox}}=0$ at low values of electron density are shown in the lower panel of Fig. 13. The peak energy of the $0\rightarrow1$ intersubband resonance at a fixed value of n_s ($\sim3.7\times10^{11}$ cm^{-2}) is essentially temperature independent over this range; the linewidth increases slightly with temperature. Near 20 K, a *second* peak becomes observable at energies above the $0\rightarrow1$ transition; this second peak moves to higher frequencies by ~12 cm^{-1} at $T=45$ K and becomes dominant for temperatures greater than 30 K. At higher values of n_s the temperature required to observe the higher-energy feature increases.

In the presence of substantial mobile positive charge these results are strongly modified. Representative differential absorption spectra for sample 1 with $\Delta N_{\text{ox}}=4.9\times10^{11}$ cm^{-2} and $n_s=4.2\times10^{11}$ cm^{-2} are shown in Fig. 14 at several temperatures. The shifted intersubband transition resonance at 4.2 K (the arrow indicates the position of the $0\rightarrow1$ transition observed at $T=4.2$ K with $\Delta N_{\text{ox}}=0$ for the same electron density) broadens, and the peak shifts rapidly to higher frequencies for temperatures between 15 and 25 K. At somewhat higher temperatures ($\gtrsim40$ K), along with further

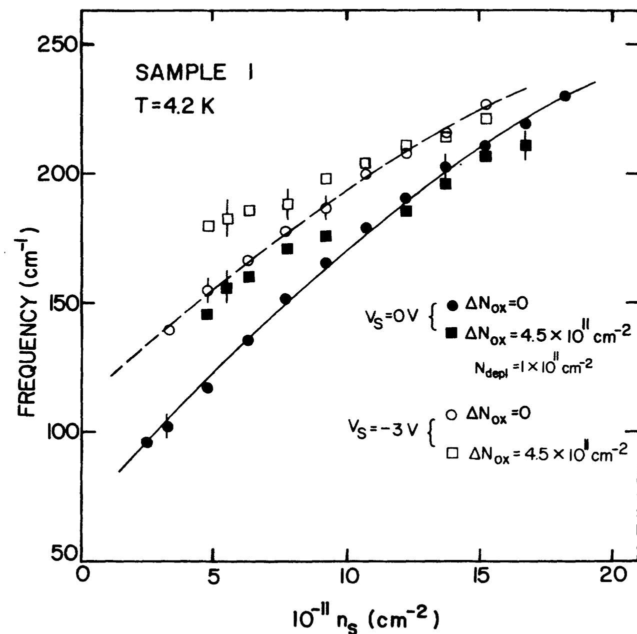

FIG. 12. Transition energy data for sample 1 at $T=4.2$ K with a negative substrate-source bias voltage for low and high values of the total positive oxide charge density (open symbols) along with results obtained with zero substrate-source bias (solid symbols). The solid and dashed lines through the respective $\Delta N_{\text{ox}}=0$ data are guides to the eye.

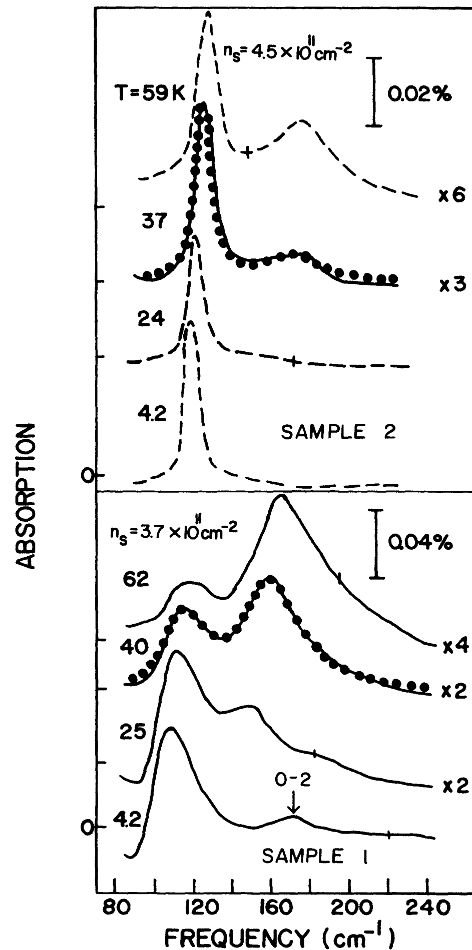

FIG. 13. Lower: Differential absorption spectra for sample 1 at temperatures between 4.2 and 77 K with $\Delta N_{\text{ox}}=0$ and $n_s=3.7\times10^{11}$ cm^{-2}. Upper: Differential absorption spectra for sample 2 at similar temperatures with $n_s=4.5\times10^{11}$ cm^{-2}. Solid circles: Lorentzian oscillator fits described in text. Bars indicate typical noise levels at high frequencies; noise levels are lower at lower frequencies.

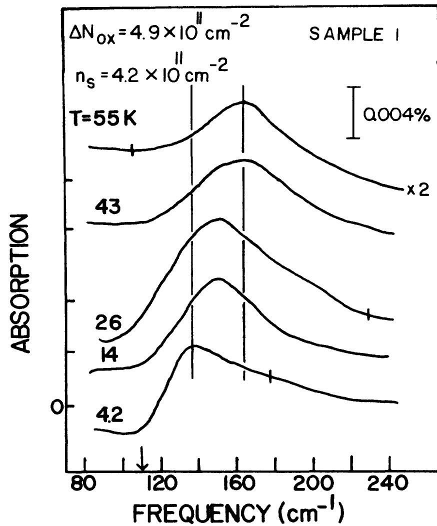

FIG. 14. Differential absorption spectra for sample 1 at temperatures between 4.2 and 77 K at a "low" value of electron density for $\Delta N_{ox}=4.9\times10^{11}$ cm^{-2}. Vertical lines indicate total shift. Arrow indicates position of the $0\rightarrow1$ transition observed at $T=4.2$ K with $\Delta N_{ox}=0$.

broadening and shifting of the peak to slightly higher energies, there appears to be some evidence of increased absorption in the frequency regime where the $0\rightarrow1$ extended-state intersubband transition should occur for this value of electron concentration. However, there is no clearly observable resonance at energies below the main broad resonance up to the maximum temperature investigated. At "high" values of n_s ($>10^{12}$ cm^{-2}) the peak energy of the resonance is essentially *temperature independent* between 4.2 and 25 K, although the line broadens significantly.

Temperature-dependent optical studies were also carried out on sample 2 at low values of electron density. Representative differential absorption spectra are shown for this device in the upper panel of Fig. 13 for several temperatures at a fixed electron concentration. Again, as for sample 1 with $\Delta N_{ox}=0$, the peak frequency of the $0\rightarrow1$ intersubband resonance is essentially temperature independent over this range. Near 40 K (approximately *twice* the temperature at which additional structure was observed in sample 1 for similar values of n_s), a *second* peak becomes observable at frequencies above (~50 cm^{-1}) the $0\rightarrow1$ transition resonance. Also, in sharp contrast to the results obtained on sample 1 for similar values of n_s and temperature, the intensity of this secondary structure remains *weaker* than the $0\rightarrow1$ intersubband resonance up to the highest temperature studied.

V. DISCUSSION

These experiments have shown that both the electrical and optical properties of electrons in Si space-charge layers are strongly affected by the presence of positive oxide charge. In order to present a coherent picture of the physics, this section is divided into three parts. In subsection A, a discussion of the general features of these results is given. The results of the electrical-transport and far-infrared measurements in the low- (subsection B) and high- (subsection C) inversion-layer electron-density regions are then discussed separately.

A. General

The results of the dc electrical-transport measurements demonstrate the significant role of the positive impurity ions as scattering centers in Si MOS devices. This can be seen most clearly by the decrease in effective mobility with increasing interfacial oxide charge density (Fig. 2). The marked decrease of the low-temperature effective mobility at high electron densities (see, e.g., $\Delta N_{ox}=0$ data in Fig. 2) is attributed to scattering due to "surface roughness;" this is characteristic of MOS devices with little net positive oxide charge near the semiconductor-oxide interface. The relatively small rate of change of effective mobility with n_s for large values of ΔN_{ox} provides evidence for the dominance of oxide charge scattering in comparison to surface-roughness scattering under these conditions.[24]

The observed broadening of the capacitance–gate-voltage curves as positive ions are drifted to the interface (Fig. 4) also demonstrates the effects of oxide charge in these devices. The significant broadening of the C-V_g curves near the minimum value (C_{min}) and slight changes in C_{min} observed at values of positive oxide charge greater than 10^{12} cm^{-2} are indicative of appreciable macroscopic lateral inhomogeneities.[20] The positive ions in this case are not randomly distributed along the Si/SiO_2 interface plane, but are pictured[25] to exist in well-separated clusters of high density separated by regions of low density. In order to avoid complications due to such inhomogeneities, the far-infrared optical measurements were confined to values of ΔN_{ox} less than approximately 7×10^{11} cm^{-2}.

The substantial difference in linewidths of the subband absorption spectra observed at 4.2 K (Fig. 8) for the poor-mobility device with $\Delta N_{ox}=0$ ($\sim$20–25 cm^{-1}) and the high-mobility device ($\sim$6–8 cm^{-1}) is also attributed to positive oxide charge scattering.[26] The broadening of the subband absorption spectra is even more pronounced (Fig. 10), as expected, in the presence of substantial interfacial oxide charge density. In spite of this, the peak position of the individual absorption lines are still clearly defined for the entire range of ΔN_{ox} investigated. It should be noted that the absolute value of the differential gate-modulation absorption signal can differ by a factor of 2–3 each time the device is mounted on the Si prism due to the variations in the bonding layer. The large loss of *integrated intensity* of the subband spectra at low values of n_s with increasing positive oxide charge in a *single run* is discussed below.

An important issue[27,28] in studies of the quasi-two-dimensional electron gas in Si MOSFET's is the accurate determination of the conductivity threshold voltage in the presence of appreciable densities of positive oxide charge at the interface. As mentioned in Sec. IV, the threshold voltages determined by conductance-voltage

measurements and capacitance-voltage measurement at 77 K in the present work are systematically different by a small amount (≤ 0.5 V) (see Table II), the I_{DS}-V_g threshold always being slightly more positive at large values of ΔN_{ox}. Threshold-determination uncertainty is the major source of error in the absolute determination of the number densities of positive oxide charge near the Si/SiO_2 interface.

B. Low electron densities

1. Electrical-transport results

The electrical-transport measurements performed on these devices with $N_{ox} \leq 4\times 10^{11}$ cm^{-2} provide evidence that the presence of positive oxide charge results in additional random surface potential fluctuations along the Si/SiO_2 interface plane and strong localization of electrons in the Si space-charge layer at low enough temperatures. Results of activated conductivity measurements performed on these samples, in which the electron density corresponding to the minimum metallic conductivity for sample 1 with $\Delta N_{ox}=0$ was found to be approximately twice the value for the clean oxide sample, demonstrate that the number density of localized states (and concomitant band-tailing effects) are greater in poorer-mobility devices, as expected.

The peaked structure observed at low temperatures before the onset of strong channel conductance for sample 1 with $\Delta N_{ox} \geq 4.0\times 10^{11}$ cm^{-2} (Fig. 3) was reported initially by Fowler and Hartstein.[8] Following these authors, this structure is attributed to the existence of a band of impurity states located below the lowest (i.e., $n=0$) subband edge associated with the twofold-degenerate subbands due to the binding of electrons to the positive ions. The disappearance of the peaked structure for large values of ΔN_{ox} ($\geq 8\times 10^{11}$ cm^{-2}) is believed to result from broadening and merging of the "impurity" band with the conduction-band tail. As noted earlier, the results of recent and more extensive dc transport experiments on similar devices[9] support the interpretation in terms of impurity bands for the range of positive oxide charge densities investigated in this study.

2. Optical results

In order to provide a simple basis for understanding the observed transition energy results versus n_s for sample 1 at 4.2 K, variational wave functions were utilized by Kramer and Wallis to describe both continuum states and the states of an electron bound to an isolated charged impurity located at or near the oxide-semiconductor interface in the presence of a constant electric field. The Hamiltonian of this model system and the form of the trial wave functions have been discussed previously.[12,16] The calculated $0\rightarrow 1$ continuum transitions in this model have been fitted to the observed $\Delta N_{ox}=0$, $0\rightarrow 1$ transition energies in order to obtain a relationship between the effective constant electric field and the inversion-layer density (F_s-n_s) for comparison with the experimental data,

$$F_s = 51.7\left[\frac{n_s}{4}+0.7\right] \text{ esu}, \tag{11}$$

where the first term is the contribution of inversion-layer electrons and the second term is the contribution of fixed ionized acceptors (both in units of 10^{11} cm^{-2}). The results for the calculated $0\rightarrow 1$ continuum intersubband transition energies are shown by the solid curve in Fig. 11. The fit is good at low values of n_s where this one-electron calculation is expected to be most accurate.

In order to generate a simple relationship between the effective constant electric field (F_s) and the inversion-layer electron density, the average separations from the interface of carriers in the ground subband derived from the Fang-Howard variational model[29] is equated to the result for the triangular well approximation,

$$F_s = 51.7(0.28n_s+0.82N_{depl}) \text{ esu}, \tag{12}$$

where n_s and N_{depl} are measured in units of 10^{11} cm^{-2}. This procedure is expected to yield a fairly accurate physical description as long as only energetically lower-lying subbands are populated; Eq. (12) is in reasonable agreement with Eq. (11), within the accuracy of the determination of N_{depl} ($\pm 15\%$).

The transition energies between the lowest bound states associated with the ground ($n=0$) and first- ($n=1$) excited subband levels $[(E_1-E_0)_B]$ have been obtained from the calculated binding energies as functions of the electric field (with the n_s-F_s relationship obtained from the $\Delta N_{ox}=0$ fit), with the distance (z_0) of the impurity ion from the interface as a parameter. This approach assumes that the measured intersubband transition energies are close to the separation between the appropriate subbands and associated bound states. Since the oscillator strengths are comparable for the bound and continuum subband transitions, it is reasonable to assume that depolarization and excitonlike corrections will be similar for both. It has been shown that these corrections nearly cancel for the present range of densities for continuum transitions.[1] The calculated energy shift of the impurity-derived intersubband transition with the impurity ion placed at the interface ($z_0=0$) is approximately twice the experimentally observed shift. With the positive ion 11 Å into the SiO_2, the dashed line plotted in Fig. 11 is obtained, consistent with results at low n_s as well as other experiments.[30] This model is clearly oversimplified, but the agreement with the present experimental results for this range of ΔN_{ox} lends support to an interpretation of the shifted lines in terms of transitions from an impurity band associated with the zeroth subband ($n=0$) to an impurity band associated with the first-excited subband ($n=1$). A schematic representation of the optical transitions (dashed arrow) between bands of impurity states associated with the two lowest-lying quantized subbands (E_0,E_1) of the twofold-degenerate conduction-band -valley system is shown in Fig. 15 along with the usual $0\rightarrow 1$ continuum intersubband transition (solid arrow). Furthermore, the oxide charge density at which the absorption lines are first shifted initially to higher energy at low n_s ($\Delta N_{ox}\sim 4\times 10^{11}$ cm^{-2}) is consistent with the ob-

servation at 4.2 K (see Fig. 3) of peaked structure before the sharp onset of conduction.

For each value of ΔN_{ox} above 4×10^{11} cm^{-2} the lines begin to approach the $\Delta N_{ox}=0$ subband transition energy curve at the value of n_s for which the onset of substantial conductance at 4.2 K is observed (Figs. 2 and 11). This is consistent with the interpretation that essentially *all* electrons induced near the interface at low temperatures are in localized states for $n_s \le N_{ox}$.

The apparent significant loss of integrated intensity of the absorption lines at low values of n_s with $\Delta N_{ox} \ge 4\times10^{11}$ cm^{-2} may result from a substantial fraction of the drifted ions being distributed over an appreciable distance in the direction perpendicular to the interface. This would lead to a broad distribution of bound-state energies skewed toward low binding energies, a further "smearing" out of the transition energies of the more weakly bound states due to substantially increased overlap of the wave functions, and concommitant difficulties in determining the baseline and thus the integrated intensity. The observed resonance peak is due to electrons bound to positive charges that are situated in a rather well-defined sheet near the interface. At high enough values of n_s, screening self-consistently reduces the binding energies of all electrons sufficiently that the majority of the impurities are ionized and the positive ions simply act as scattering centers for the electrons in "extended" states.

As noted previously, experimentally observed shifts with oxide charge density of the subband resonance for *n*-type accumulation layers in Si MOSFET's have been interpreted in terms of a self-energy shift in a memory-function approach due to increased scattering in the *absence* of an impurity band.[17] Gold has taken the value of depletion charge density ($N_{depl}=1\times10^{11}$ cm^{-2}) and range of N_{ox} investigated in the present study and calculated the expected dependence of the intersubband resonance energy on electron density with this model.[31] For $n_s=5\times10^{11}$ cm^{-2} this theory predicts a monotonically increasing shift to higher energies of the maximum of the frequency-dependent conductivity associated with the $0\rightarrow1$ transition. The present experimentally observed shift is *independent* of ΔN_{ox} over this range (see Fig. 11). In addition, for $\Delta N_{ox} < (3-4)\times10^{11}$ cm^{-2} and comparable values of n_s, the experiments show *no* shift of the subband absorption peak contrary to these predictions.

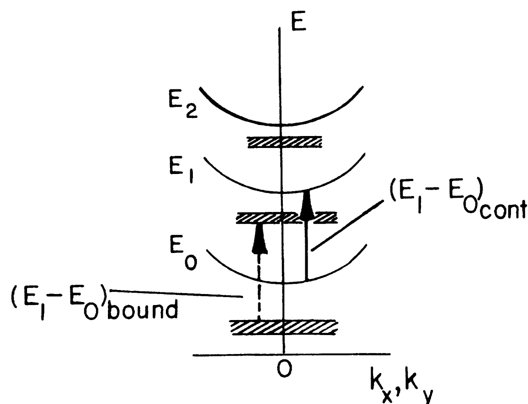

FIG. 15. Schematic representation of optical transitions between bands of impurity states (dashed arrow) associated with the lowest-lying quantized subbands (E_0,E_1) and the usual $0\rightarrow1$ continuum intersubband transition (solid arrow).

A unique advantage of the Si MOSFET device is that the net surface electric field can be varied via substrate-source bias voltages, while keeping n_s unchanged. With $V_S=-3$ V and $n_s=4.5\times10^{11}$ cm^{-2} (Fig. 12), the equilibrium depletion charge density is twice the value with $V_S=0$ V, but the effective electric field [Eq. (11)] increases by only 35% ($100\rightarrow135$ esu). The calculated energy difference between the impurity-shifted intersubband transition $[(E_1-E_0)_B]$ and the continuum $0\rightarrow1$ intersubband transition $[(E_1-E_0)_G]$ at these two values of electric field is very small, in agreement with experimental observation at low values of n_s (The absolute values differ by a factor of 2 from the measured values since the impurity ion is assumed to be *at* the interface in these calculations).

The qualitative behavior of the peak energy of the $0\rightarrow1$ intersubband resonance with temperature (i.e., essentially temperature independent) for the poor-mobility sample with $\Delta N_{ox}=0$ and the clean oxide device (Fig. 13) is in qualitative agreement with a recent calculation[32] for the same temperature range and low values of n_s ($<10^{12}$ cm^{-2}). The second peak observed from measurements on sample 1 above 10 K (whose intensity grows with increasing temperature) at the lowest electron concentration investigated in this study is attributed to transitions ($0'\rightarrow1'$) originating in the ground subband states of the energetically higher-lying fourfold-degenerate conduction-band valleys (primed subbands), which become populated at elevated temperatures. Similar results have been previously reported from temperature-dependent intersubband resonance optical studies on "clean" oxide MOS devices.[33] The shift to higher frequencies of the $0'\rightarrow1'$ transition resonance with temperature is consistent with calculations[33] at finite temperature; the positive energy shift of the peak at the higher temperatures is attributed to the exchange lowering of the $0'$ quasiparticle states as more electrons thermally occupy these states. The present results provide evidence that electron-electron interactions (i.e., many-body effects) have larger effects on the primed subbands[34] than on the unprimed subbands due to the larger in-plane effective mass ($m'_{\parallel}/m_{\parallel}=2.2$) and higher valley degeneracy ($g'_v/g_v=2$).

The energy of the ground ($E_{0'}$) subband for the upper valleys has been calculated in an extended-state model for this range of electron density[35] and found to be very close (15–20 meV) to the E_1 subband energy for the lower valleys. Thus, the observation of intersubband transitions associated with the upper valleys at such low temperatures ($k_BT\sim2$ meV) is unexpected for extended states; rather, it is likely that localized states associated with $E_{0'}$ extend to substantially lower energies than the $E_{0'}$ edge and, hence, the transitions originate in these localized

"tail" states.

The temperature-dependent studies on the "clean" oxide MOSFET device were performed to test this assertion. As seen from a direct comparison of the absorption spectra (Fig. 13), the relative intensities of the $0 \rightarrow 1$ and $0' \rightarrow 1'$ intersubband transitions for these two devices for similar values of n_s and temperature are *considerably* different.

In order to extract the 0-0′ energy separations from these data, the functional form of the dynamical transverse conductivity is taken to be a Lorentzian,

$$F(x) = A \left[\frac{\varepsilon}{(x - x_0)^2 + \varepsilon^2} \right] , \tag{13}$$

where A is the amplitude and ε is the half-width at half maximum. The line intensities of these data are fitted as the sum of two Lorentzian oscillators that describe, respectively, the $0 \rightarrow 1$ and $0' \rightarrow 1'$ intersubband transition resonances. Representative fits, with the amplitudes (A, A') and half-widths $(\varepsilon, \varepsilon')$ of the individual resonances as adjustable parameters, are plotted as the solid circles in Fig. 13. From a comparison of the real part of the dynamical transverse conductivity at resonance with the value of $F(x)$ at $x = x_0$ for the $0 \rightarrow 1$ and $0' \rightarrow 1'$ intersubband transitions, the ratio of the number densities of electrons in the E_0 and $E_{0'}$ subbands is obtained. Variational wave functions of the Fang-Howard type were employed to determine approximately the ratio of the dipole matrix elements for the respective transitions along with the fact that the values of the variational parameters of the envelope wave functions associated with the ground and first-excited subbands are approximately equal for the range of surface electric fields investigated ($10^4 - 10^5$ V/cm).[36]

The relative occupation of the levels was separately determined with a three-subband extended-state model (E_0, $E_{0'}$, and E_1). The fixed total electron density is given by

$$\begin{aligned} n_s &= n_0 + n_{0'} + n_1 \\ &= \int_{E_0}^{\infty} f(E)\rho(E)dE + \int_{E_{0'}}^{\infty} f(E)\rho'(E)dE \\ &\quad + \int_{E_1}^{\infty} f(E)\rho(E)dE , \end{aligned} \tag{14}$$

where all energies are measured relative to the E_0 subband level, $f(E)$ is the Fermi-Dirac distribution function, and the ratio between the density of states per unit energy per unit area associated with the respective subband systems is

$$\frac{\rho'(E)}{\rho(E)} = 4.39 . \tag{15}$$

An expression is derived for the $E_{0'}$ subband energy in terms of the chemical potential, μ, and the three known parameters (T, $E_1 - E_0$, and n_s); μ is varied over a range of values, and $n_0/n_{0'}$ is determined for each $(\mu, E_{0'})$ pair. Comparing the relative occupation factors obtained from the fits described above with these results gives 0-0′ energy separations for the "clean" sample in good agreement with the theoretical calculations (0-0′ separation ~ 14 meV). On the contrary, similar fits for sample 1 with $\Delta N_{ox} = 0$ yield *very small* apparent 0-0′ energy separations ($\sim \frac{1}{3}$ of those predicted). From this comparison it is concluded that the small *apparent* 0-0′ separations obtained with an extended-state model are a result of long band tails (ignored in the extended-state model) associated with the E_0 and $E_{0'}$ subbands which greatly modify the density of states of these subbands. Since the functional form of these "band tails" is not known, and an *ad hoc* assumption of a form with adjustable parameters would not add significantly to the physical understanding of this system, no such fits were attempted.

Similar analyses for sample 1 with $\Delta N_{ox} = 0$ at higher carrier concentration yield, as expected within an extended-state model, larger 0-0′ energy separations (but still only approximately one-half of those predicted). In addition, the increase in relative intensity of the $0' \rightarrow 1'$ intersubband resonance observed for the high-mobility device with positive substrate-source bias voltages compared to the results obtained with $V_S = 0$ V for the same electron density is consistent with the smaller 0-0′ energy separation expected under these conditions. A summary of the 0-0′ energy separations determined from analyses of representative absorption spectra is presented in Table III for both devices.

The results are strongly altered in the presence of substantial positive oxide charge (Fig. 14) at low electron densities ($n_s < N_{ox}$). The rapid shift to higher frequencies of the transition resonance peak with temperature is ascribed to unresolved contributions to the overall line profile from impurity-shifted subband transitions; these transitions result from populating *bound states* (an impurity band) associated with the ground subband of the upper, fourfold-degenerate conduction-band valleys. This is an assertion; it cannot be concluded from these measurements alone due to the very broad lines observed. However, the observed shift is qualitatively consistent with the results of a recent calculation performed by Kramer and Wallis[36] of the transition energies for electric dipole transitions between impurity states associated with the two lowest-lying primed subbands. These calculations indicate that the energy difference between impurity states of the two lowest-lying subbands associated with

TABLE III. Summary of the 0-0′ energy separations extracted from analyses of differential absorption spectra at temperatures between 4.2 and 77 K. The $0 \rightarrow 1$ transition energies are determined directly from the positions of the subband absorption peaks.

Sample	n_s (cm^{-2})	T (K)	$E_1 - E_0$ (meV)	$E_{0'} - E_0$ (meV)
1	3.7×10^{11}	40	14.3	7.2 ± 1
1	3.7×10^{11}	62	14.5	5.7 ± 1
1	6.0×10^{11}	30	17.9	8.6 ± 1
1	7.5×10^{11}	42	20.5	8.0 ± 1
2	4.5×10^{11}	59	15.9	14.9 ± 2
2	4.5×10^{11}	57	13.9	10.4 ± 2

the upper valleys $[(E_{1'}-E_{0'})_B]$ is greater than the corresponding energy difference associated with the lower subband system $[(E_1-E_0)_B]$ for this range of surface electric fields. Thus, the interpretation of the temperature-dependent subband measurements obtained for sample 1 with substantial interfacial oxide charge density $[\Delta N_{ox}=(3-4)\times 10^{11}\ \mathrm{cm}^{-2}]$ at low n_s is at least plausible in light of these calculations.

This interpretation is also consistent with field-effect–mobility data taken on the same samples (Fig. 5). The peaked structure observed at low gate voltages at 4.2 K above a minimum value of positive oxide charge density $[\Delta N_{ox}>4\times 10^{11}\ \mathrm{cm}^{-2}$; see, e.g., Fig. 5(c)] corresponds to a maximum of the slope of σ versus V_g (i.e., $\partial\sigma/\partial V_g$) due to the band of impurity states below the E_0 subband (compare with Fig. 3). The second peaked structure which rapidly develops at higher gate voltage with increasing temperature above 10 K is attributed to the population of bound states associated with the ground subband ($E_{0'}$) of the higher-lying valleys which modifies the conductivity and its derivative. This additional sharp feature for temperatures *slightly* higher than 4.2 K was *not* observed in measurements taken on the high-mobility samples (Fig. 7). However, a peaked structure is observed near 77 K at gate voltages slightly above threshold [as also observed for sample 1 with $\Delta N_{ox}=0$, Fig. 5(a)]. Similar structure was reported some time ago on a nominally uncontaminated sample;[37] no explanation was offered for the appearance of the peaks. It has been suggested[1] that this structure may arise from electron-transfer effects similar to those observed in samples where uniaxial stress was employed to make $E_{0'}<E_0$ at low n_s.[38] The present far-infrared measurements obtained for both large-gate-area devices at 4.2 K and above are not consistent with crossover of the 0 and 0′ continuum subband levels due to intrinsic strains in the semiconductor-insulator junction since the field-effect–mobility structure observed for sample 1 at 4.2 K and above *clearly* depends on ΔN_{ox}.

Tidey and Stradling have reported[39] extensive structure in the variation of field-effect mobility with gate voltage near the threshold voltage at temperatures above 20 K for n-type inversion layers in "high-quality" p-type Si MOS devices (with substrate resistivity $\sim 10\,000\ \Omega\,\mathrm{cm}$). The qualitative features of these results were simulated with the aid of the usual two-dimensional density-of-states model with the addition of discrete localized states (the peaked structure was attributed to a thermally activated change in free charge) with small binding energies ($\sim$10–20 meV) below the E_0 band edge; the source of these trap states was postulated to be positive oxide charge at or near the Si/SiO_2 interface. A somewhat related interpretation may be appropriate for the present temperature-dependent field-effect–mobility measurements, but with activation from localized states below $E_{0'}$ as well as below E_0. The results are difficult to simulate for sample 1 (no such fits were attempted) since the functional forms of the band tails and "impurity bands" associated with the twofold- and fourfold-degenerate subband systems are not known.

These results, together with the observation at *similar* elevated temperatures of impurity-derived transitions associated with the higher subband states ($E_{0'}, E_{1'}$) from the higher-lying valleys for $\Delta N_{ox}>4\times 10^{11}\ \mathrm{cm}^{-2}$ at low n_s, are consistent with a model of localized states in long band tails extending well below the mobility edges, and the formation of impurity bands for *both* sets of valleys above a minimum value of added positive oxide charge density $[\Delta N_{ox}\sim(3-4)\times 10^{11}\ \mathrm{cm}^{-2}]$. Based on the above, a qualitative picture of the density of states in the presence of substantial positive oxide charge density is presented in Fig. 16 for this proposed model; band tails and "impurity" bands associated with the lowest subbands (E_0 and $E_{0'}$) from both sets of conduction-band valleys are shown.

C. High electron densities

In the high-electron-density region where the transition energies of the shifted lines are coincident within ex-

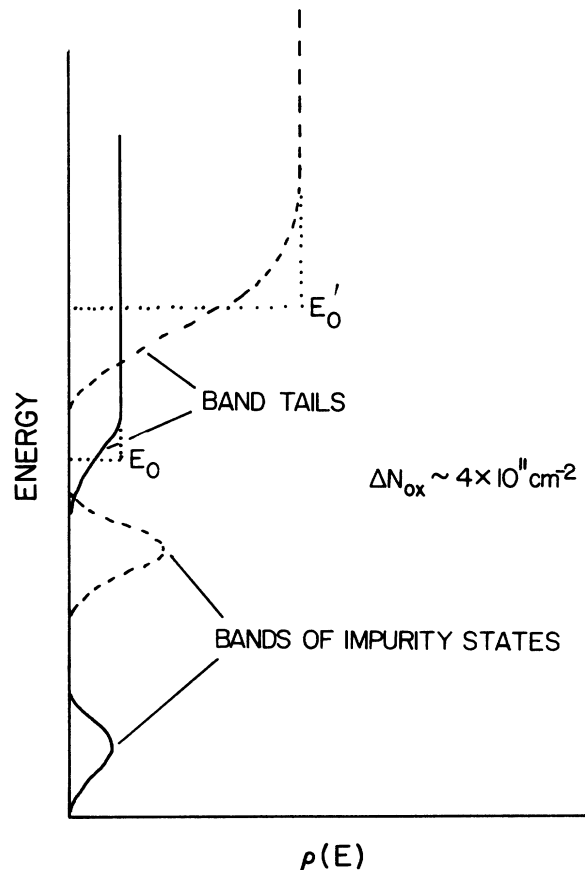

FIG. 16. Schematic density of states in the presence of a large density of positive oxide charge as described in text. Band tails and "impurity bands" associated with the E_0 subband (solid lines) and the $E_{0'}$ subband (dashed lines) are shown. Dotted curves are the respective ideal band edges.

perimental error with the $\Delta N_{ox}=0$ subband transition energies, it appears that there is strong screening of the positive ions by the excess mobile electrons in the inversion layer. The effective binding energy of electrons to the positive ions becomes very small with $n_s \geq 2N_{ox}$, resulting in essentially all impurities being ionized even at 4.2 K (small binding energies are predicted by Vinter[13] for the case in which the number of inversion-layer electrons is *much larger* than the number of interfacial impurity ions). Thus, it is concluded that these data provide direct optical evidence of screening of localized states in quasi-two-dimensional systems. The optical transition at *high* enough inversion-layer electron densities can be described in terms of the usual subband transitions in the presence of a large density of screened Coulomb scattering centers. Furthermore, in this region of high electron density, the frequency positions of the resonance peaks are essentially *independent* of oxide charge, while there is a substantial broadening of the lines with increasing oxide charge. The broadening of the resonance lines and the correlation between the line widths and effective mobilities has been previously reported.[26]

The shifted intersubband transition resonance energies calculated by Gold at low values of electron density approach and eventually are close to the unperturbed ($\Delta N_{ox}=0$) subband curve at high carrier concentration ($n_s \geq 15\times 10^{11}$ cm^{-2}), in qualitative agreement with the present results. Thus, the model used by Gold (no impurity band) is consistent with the present measurements at *high values* of n_s, but not at low values of n_s. It is more likely to be generally appropriate to the case of accumulation layers, since there is little depletion field and the binding energies are much smaller than the present case, and would be rapidly reduced with n_s by screening.

VI. SUMMARY AND CONCLUSIONS

Systematic studies of electrical conductivity and far-infrared absorption of electrons in inversion layers in Si MOSFET's have been carried out in order to investigate localization effects in quasi-two-dimensional systems. Devices in which positive impurity ions were controllably drifted to the oxide-semiconductor interface as well as devices with "clean" oxides were investigated.

Electrical conductance as a function of gate voltage in Si MOSFET's for various number densities of mobile positive ions (ΔN_{ox}) drifted to the Si/SiO_2 interface showed at 77 K threshold voltage shifts, as expected, to larger negative values as ΔN_{ox} was increased. At low temperatures ($\sim$4.2 K) the peak effective mobility was found to decrease with increasing ΔN_{ox}. Furthermore, for $\Delta N_{ox} > 4\times 10^{11}$ cm^{-2}, a peak in conductance appears at a more negative gate voltage than that for which the sharp onset in conductance occurs; this conductance "bump" is attributed to the formation of a well-defined impurity band. In addition, field-effect–mobility measurements as a function of temperature exhibit peaked structure whose complexity increased with ΔN_{ox}.

At low values of N_{ox} far-infrared absorption lines were observed at 4.2 K that, over the whole range of n_s investigated, correspond to the usual extended-state intersubband ($0\rightarrow 1$) transitions. The $0\rightarrow 1$ transition energies are in good agreement with recent many-body calculations of the subband structure in n-type inversion layers. The transition frequencies as a function of electron density remain unchanged with increasing N_{ox} up to $\sim 4\times 10^{11}$ cm^{-2}. At larger values of oxide charge, and over a range of (low) inversion-layer electron densities, the absorption lines are shifted to higher energy by about 4 meV, *independent* of N_{ox}. As n_s is increased beyond N_{ox}, the transition energies of the shifted lines approach the extended-state subband transition energies and are coincident with this curve within experimental error for n_s greater than approximately $2N_{ox}$. At temperatures greater than 20 K and at low values of n_s and N_{ox}, a second peak appears at a higher frequency than that of the primary peak. The introduction of a substantial number density of mobile positive ions at the interface with $n_s < N_{ox}$ broadens both peaks at the higher temperatures.

The shift in the intersubband transition frequencies at low temperatures for low values of n_s in the presence of substantial positive oxide charge is due to the localization of the electrons on the ions. Bound states are created below the $n=0$ and 1 subbands with the binding energy associated with the $n=0$ subband greater than that associated with the $n=1$ subband. The absorption lines shifted to higher frequencies at low n_s are attributed to bound intersubband transitions from an impurity band associated with $n=0$ to an impurity band associated with $n=1$. The frequency is shifted by the difference in binding energies. This interpretation is consistent with recent calculations of impurity-shifted intersubband transitions and is in contrast with the predictions of a recent theoretical model of observed shifts in terms of a self-energy correction due to increased scattering in the *absence* of an impurity band. Several features of the experimental results argue against the latter interpretation.

As the electron concentration increases beyond N_{ox}, the binding energies decrease rapidly due to screening, thus leading to the coalescence of the curves for $n_s \geq 2N_{ox}$. To our knowledge this represents the first *direct* evidence via optical experiments of the effects of screening on localized electronic states. In addition, at high inversion-layer electron densities the intersubband resonance linewidths as a function of positive oxide charge density are found[38] to be correlated with the corresponding scattering rates determined from the effective mobilities. This result is in good agreement with a calculation for short-range scatterers.

The additional peak at elevated temperatures for low values of n_s and N_{ox} is attributed to transitions ($0'\rightarrow 1'$) originating in the ground subband states of the energetically higher-lying fourfold-degenerate conduction-band valleys. Analyses of these data yield *very small* apparent 0-0′ energy separations for the poor-mobility Si MOS device. On the other hand, similar analyses for the "clean" oxide device give 0-0′ energy separations in good agreement with theoretical calculations. This apparent contradiction is attributed to the existence of long band tails associated with both the E_0 and $E_{0'}$ subbands in poorer-

quality samples. In the presence of substantial positive oxide charge density (i.e., $N_{ox} \geq 4\times 10^{11}$ cm^{-2}) the rapid shift of the peak to higher frequencies at low n_s and for temperatures greater than ~ 15 K is ascribed to unresolved contributions due to populating *bound states* (an impurity band) associated with the $E_{0'}$ subband. This picture is consistent with the results of a recent calculation[36] of the energy difference between impurity states of the lowest-lying two subbands associated with the upper valleys.

These studies suggest several extensions. Effects of a high magnetic field on the binding energy should be observable and should permit an improved understanding of the impurity band in such confined systems to be achieved. In addition to the lowest impurity band associated with the ground subband in the inversion layer with $N_{ox} \geq 4\times 10^{11}$ cm^{-2}, excited impurity bands (corresponding to the excited states of an impurity) also exist in this structure. Electric dipole optical transitions between ground and excited impurity bands are allowed and should be observable with the ir electric field vector polarized in the plane of the interface. Observation of the ground- to excited-state impurity-band transitions associated with the lowest confinement subband will provide unambiguous evidence of the existence of the impurity band and a more precise determination of the binding energy and its dependence on electric field (confinement) and electron density (screening). This should also permit a detailed spectroscopic investigation of the metal-insulator transition to be carried out in this nearly-2D system.

ACKNOWLEDGMENTS

This work was supported in part by the U.S. Office of Naval Research under Contract No. N0001483-K-0219. The authors are grateful to L. R. Cooper for his continued support and encouragement. Thanks are also due R. Czaputa for important contributions in the early stages of this work, to G. Kramer and R. F. Wallis for continuing discussions and providing theoretical results prior to publication (preceding paper), to A. Gold for discussions and providing unpublished results appropriate to the present experimental situation, and to F. Koch for helpful discussions and comments. The MOS devices used in these studies were fabricated by the U.S. Naval Research Laboratory Microelectronics Facility under the expert guidance of P. Reid.

---

*Present address: Naval Research Laboratory (Code 6870), Washington, D.C. 20375-5000.

[1]T. Ando, A. B. Fowler, and F. Stern, Rev. Mod. Phys. **54**, 437 (1982).

[2]A. Hartstein and A. B. Fowler, Phys. Rev. Lett. **34**, 1435 (1975).

[3]B. D. McCombe and D. E. Schafer, *Proceedings of the XIVth International Conference on the Physics of Semiconductors, Edinburgh, 1978,* Inst. Phys. Conf. Ser. No. 43 (IOP, London, 1979), p. 1227.

[4]A. Gold. W. Götze, C. Mazure, and F. Koch, Solid State Commun. **49**, 1085 (1984).

[5]A preliminary report of this work was presented in E. Glaser, R. Czaputa, and B. D. McCombe, Phys. Rev. Lett. **57**, 893 (1986).

[6]F. Stern and W. E. Howard, Phys. Rev. **163**, 816 (1967).

[7]N. F. Mott, Philos. Mag. **13**, 989 (1966).

[8]A. B. Fowler and A. Harstein, Philos. Mag. B **42**, 949 (1980).

[9]G. Timp, A. B. Fowler, A. Hartstein, and P. N. Butcher, Phys. Rev. B **34**, 8771 (1986).

[10]B. Vinter, Solid State Commun. **28**, 861 (1978).

[11]N. O. Lipari, J. Vac. Sci. Technol. **15**, 1412 (1978).

[12]B. G. Martin and R. F. Wallis, Phys. Rev. B **18**, 5644 (1978).

[13]B. Vinter, Phys. Rev. B **26**, 6808 (1982).

[14]O. Hipólito and V. B. Campos, Phys. Rev. B **19**, 3083 (1979).

[15]W. Kohn and L. J. Sham, Phys. Rev. **140**, A1133 (1965).

[16]G. M. Kramer and R. F. Wallis, Surf. Sci. **113**, 148 (1982), and references therein.

[17]C. Mazure, F. Martelli, A. Gold, V. Grzesik, H. R. Chang, and F. Koch, Solid State Commun. **54**, 443 (1985).

[18]A. Gold, Phys. Rev. B **32**, 4014 (1985).

[19]S. M. Sze, *Physics of Semiconductor Devices* (Wiley, New York, 1981), Chaps. 7 and 8.

[20]E. H. Nicollian and J. R. Brews, *MOS (Metal-Oxide-Semiconductor Physics and Technology* (Wiley, New York, 1982).

[21]W. J. Moore and H. Shenker, Infrared Phys. **5**, 99 (1985). The authors are grateful to Dr. W. J. Moore and Mr. E. Swiggard for the bulk Ge:Ga material and to Dr. H. Dietrich for ion implantation of boron for the Ohmic contacts.

[22]B. D. McCombe, R. T. Holm, and D. E. Schafer, Solid State Commun. **32**, 603 (1979).

[23]T. Ando, Z. Phys. B **26**, 363 (1977).

[24]See, also, A. Hartstein, A. B. Fowler, and M. Albert, Surf. Sci. **98**, 181 (1980).

[25]T. H. DiStefano, Appl. Phys. Lett. **19**, 280 (1971).

[26]E. Glaser, R. Czaputa, and B. D. McCombe, Solid State Commun. **54**, 715 (1985).

[27]A. B. Fowler and A. Hartstein, Surf. Sci. **98**, 169 (1980).

[28]J. E. Furneaux and T. L. Reinecke, Phys. Rev. B **33**, 6897 (1986).

[29]F. F. Fang and W. E. Howard, Phys. Rev. Lett. **16**, 1977 (1966).

[30]D. J. DiMaria, J. Appl. Phys. Lett. **48**, 5149 (1977).

[31]A. Gold (private communication).

[32]S. Das Sarma, R. K. Kalia, M. Nakayama, and J. J. Quinn, Phys. Rev. B **19**, 6397 (1979).

[33]P. Kneschaurek and J. F. Koch, Phys. Rev. B **16**, 1590 (1977).

[34]S. Das Sarma and B. Vinter, Phys. Rev. B **26**, 960 (1982).

[35]B. Vinter, Phys. Rev. B **15**, 3947 (1977).

[36]G. Kramer and R. F. Wallis, preceding paper, Phys. Rev. B **37**, 10 764 (1988).

[37]F. F. Fang and A. B. Fowler, Phys. Rev. **169**, 619 (1968).

[38]See, for example, I. Eisele, Surf. Sci. **73**, 315 (1978).

[39]R. J. Tidey and R. A. Stradling, J. Phys. C **7**, L356 (1974).